ACS SyntheticBiology

pubs.acs.org/synthbio

Research Article

Characterizing and Controlling Nanoscale Self-Assembly of Suckerin-12

Jasmine M. Hershewe, William D. Wiseman, James E. Kath, Chelsea C. Buck, Maneesh K. Gupta, Patrick B. Dennis, Rajesh R. Naik, and Michael C. Jewett*

Cite This: *ACS Synth. Biol.* 2020, 9, 3388–3399

Read Online

ACCESS | Metrics & More | Article Recommendations | Supporting Information

ABSTRACT: Structural proteins such as "suckerins" present promising avenues for fabricating functional materials. Suckerins are a family of naturally occurring block copolymer-type proteins that comprise the sucker ring teeth of cephalopods and are known to self-assemble into supramolecular networks of nanoconfined β-sheets. Here, we report the characterization and controllable, nanoscale self-assembly of suckerin-12 (S12). We characterize the impacts of salt, pH, and protein concentration on S12 solubility, secondary structure, and self-assembly. In doing so, we identify conditions for fabricating ~100 nm nanoassemblies (NAs) with narrow size distributions. Finally, by installing a noncanonical amino acid (ncAA) into S12, we demonstrate the assembly of NAs that are covalently conjugated with a hydrophobic fluorophore and the ability to change self-assembly and β-sheet content by PEGylation. This work presents new insights into the biochemistry of suckerin-12 and demonstrates how ncAAs can be used to expedite and fine-tune the design of protein materials.

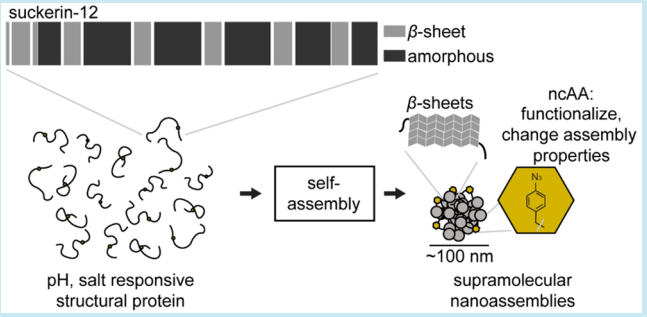

KEYWORDS: *protein nanomaterials, self-assembly, suckerins, bioinspired materials, protein characterization, noncanonical amino acids*

Self-assembling and stimulus-responsive proteins hold promise for engineering functional materials and nanomedicines.[1−6] With an exact sequence control, stimuli responsiveness, and biocompatibility, block copolymer proteins, such as elastin-like polypeptides, silk fibroins, and the recently discovered "suckerins", are of particular interest for fabricating materials.[7−15] Additionally, the ability to incorporate noncanonical amino acids (ncAAs) into protein materials has further expanded their functionality.[16−22] The suckerins are a family of structural proteins that make up the sucker ring teeth (SRT), a circular structure with hook-like teeth located in the arms of cephalopods that assist in wrangling prey.[13] With an elastic modulus on the order of GPa, SRT rival synthetic polymers in strength despite the absence of nature's common hardening methods like biomineralization and cross-linking.[23] Rather, the mechanical strength of SRT is derived from weak protein−protein interactions that stabilize a semicrystalline protein mesh that is mechanically reinforced by precisely sized nanoscale β-sheets.[13,24,25] Suckerins have conserved, modular, diblock copolymer architectures that consist of β-sheet domains flanked by aromatic-rich amorphous domains. This architecture is intimately linked to the emergent supramolecular assembly of suckerins, permitting (i) formation of H-bond networks with inter- and intramolecular β-sheets and (ii) $\pi-\pi$ stacking of aromatic residues in distally located amorphous domains.[26,27]

While the modular architecture of suckerins plays key roles in the assembly, strength, and processing of natural SRT, the structural and physiochemical properties of recombinant suckerin proteins and peptides have been exploited to make synthetic materials.[11,27,28] Building upon a robust field of work with β-sheet-rich silk fibroins, Miserez and others have pioneered the design of suckerin-based functional materials, including substrates for metallic nanoparticle growth,[29] underwater adhesives,[18] and cross-linked hydrogels.[30,31] Being of key importance for the present work, the histidine (His)-rich 39-kDa suckerin-19 (S19) was recently shown to assemble into stable, β-sheet-rich nanoassemblies (NAs).[32] S19, where the number 19 refers to the isoform number, is the most thoroughly characterized suckerin isoform to date.[11] This work established that recombinant S19, which naturally forms polydisperse colloids in aqueous solution upon purification, can be controllably assembled into relatively monodispersed NAs of a range of sizes.[32,33] Self-assembly was achieved using a salting-out method where a simple manipulation of solvent pH

Received: August 22, 2020
Published: November 17, 2020

https://dx.doi.org/10.1021/acssynbio.0c00442
ACS Synth. Biol. 2020, 9, 3388–3399

and ionic strength led to a controllable chain collapse, β-sheet formation, and subsequent self-assembly of NAs. The densely packed β-sheets in S19 NAs enabled the noncovalent encapsulation of DNA and hydrophobic small molecules, while the high His content enabled pH-dependent intracellular cargo release in mouse models.[32] These results set a precedent for how the unique features of suckerins can be leveraged to fabricate functional nanocarriers for biomedical applications or in other functional materials. Additionally, since suckerins are proteins, they are amenable to the incorporation of ncAAs. ncAAs expand the functionality of proteins by increasing the available chemical diversity of amino acids.[34,35] Of particular importance to this work, ncAAs can be used for the efficient and site-specific biorthogonal functionalization of proteins.[22,36] This provides advantages over traditional lysine or cysteine labeling because the labeling reaction has no crosstalk with native amino acids.

As they are crucial parameters in the engineering of nanocarriers,[37] we sought to access new suckerin NA particle sizes and compositions in this work. Suckerin proteins range in size (~5−60 kDa), isoelectric point (pI ~ 7−10), relative proportion and spacing of repeat domains, and the number of repeat units within the protein sequence.[24] Since the amino acid sequence dictates the stability, geometry, and presentation of β-sheets, which are critical for self-assembly, the family of suckerins are a potential toolbox for making NAs with tunable sizes and pH responses.

In this study, we report the biochemical characterization and controllable self-assembly of the 23 kDa suckerin-12 (S12). S12 has a similar architecture and sequence to S19, including a His-rich primary sequence, yet is a smaller, more soluble protein. With an eye toward controllable self-assembly, we manipulate solvent conditions to controllably unfold and refold β-sheets in S12. By varying salting-out process conditions (pH, salt type, protein concentration, and ionic strength), we identify conditions for salting out ~100 nm NAs with narrow size distributions. Additionally, we show that S12 can be efficiently expressed and purified with a ncAA handle for site-specific, biorthogonal functionalization. We use the ncAA to covalently prefunctionalize S12 with a small, hydrophobic fluorophore before self-assembly, resulting in fluorophore-loaded NAs without the need to change self-assembly conditions. Finally, we show that altering the hydrophobicity of S12 through PEGylation changes the self-assembly and β-sheet enrichment. Taken together, this work presents new biochemical characterizations of S12 and shows the utility of ncAAs to accelerate the building and testing new protein materials.

RESULTS AND DISCUSSION

Expression, Characterization, and Biorthogonal Functionalization of S12. The block copolymer architecture and amino acid sequence of S12 are shown in Figure 1A, highlighting several important biochemical features. S12 comprises six repeats of β-sheet forming blocks flanked by amorphous blocks. β-sheet blocks are alanine rich, resembling β-sheet-forming domains in silk fibroin,[38] and amorphous blocks are glycine (Gly) and tyrosine (Tyr) rich. Importantly, for controlled assembly and mechanical strength, β-sheet regions are flanked by proline residues, confining β-sheets to specific nanoscale dimensions.[27] The high Tyr content of amorphous blocks (15% by mol) plays an important role in the supramolecular arrangement of suckerins *via* aromatic π−π

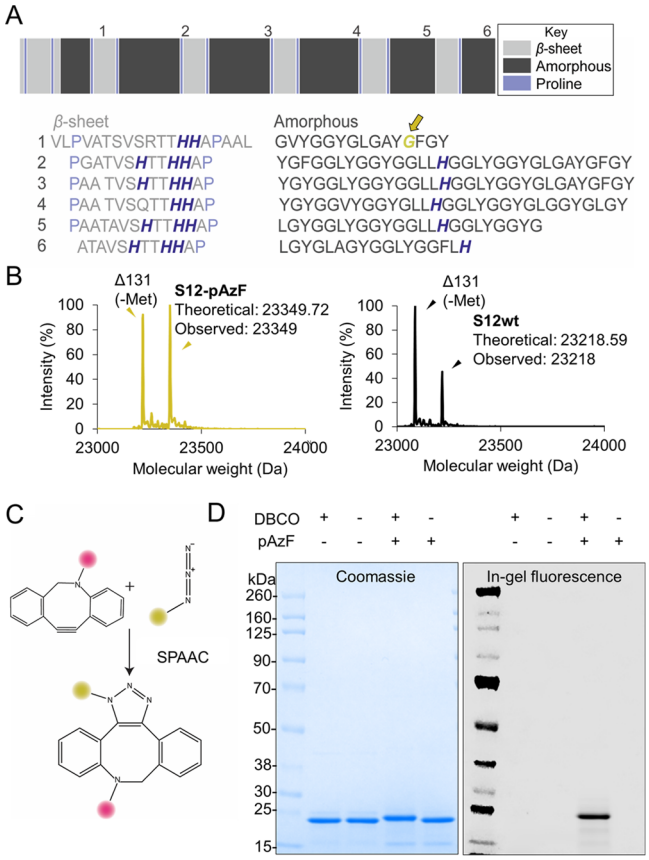

Figure 1. Expression, characterization, and biorthogonal functionalization of S12. (A) Schematic of block copolymer architecture of S12 (top). Left to right is N- to C- terminus. Amino acid sequence of S12, with the six repeats of β-sheet and amorphous blocks shown (bottom). Histidine residues are colored in dark purple. Gly 32, which was mutated to pAzF (S12-pAzF), is highlighted in gold and annotated with a gold arrow. (B) Deconvoluted liquid chromatography mass spectra of S12-pAzF (left) and S12wt (right). Mass signatures corresponding with methionine-cleaved proteins are indicated. (C) Strain-promoted azide−alkyne cycloaddition (SPAAC) for biorthogonal coupling. The azido protein is represented as a gold circle, and the DBCO-labeled partner is represented as a pink circle. (D) SDS-PAGE analysis of protein purity and SPAAC reactions. A Coomassie stain is shown in left, and the in-gel fluorescence of the DBCO-TAMRA probe conjugated to S12 is shown in right. −pAzF and +pAzF refer to S12wt and S12-pAzF, respectively. Data are representative of three independent experiments.

stacking interactions that orient and stabilize distal amorphous domains. From a practical perspective, the high Tyr content also enables interprotein di-Tyr cross-linking of β-sheet enriched monomers for stabilizing nanocarriers for downstream use.[30,32] S12 is hydrophobic in character but contains 9 mol % His. The protonation of His residues is thus important for solubility, conferring high solubility of up to 60 mg/mL in slightly acidic conditions (~pH 5).[30]

We overexpressed and purified wild-type S12 (S12wt) and a point mutant of S12 bearing a single ncAA from *Escherichia coli*-based cultures. To enable biorthogonal functionalization, we replaced the native Gly residue at position 32 with the ncAA para-*L*-azido-phenylalanine (pAzF), referred to as S12-pAzF. To choose a site for ncAA incorporation, we tested the incorporation of pAzF at seven locations in the protein: Gly 32, Gly 59, phenylalanine (Phe) 77, Gly 101, Phe 121, Gly

https://dx.doi.org/10.1021/acssynbio.0c00442
ACS Synth. Biol. 2020, 9, 3388−3399

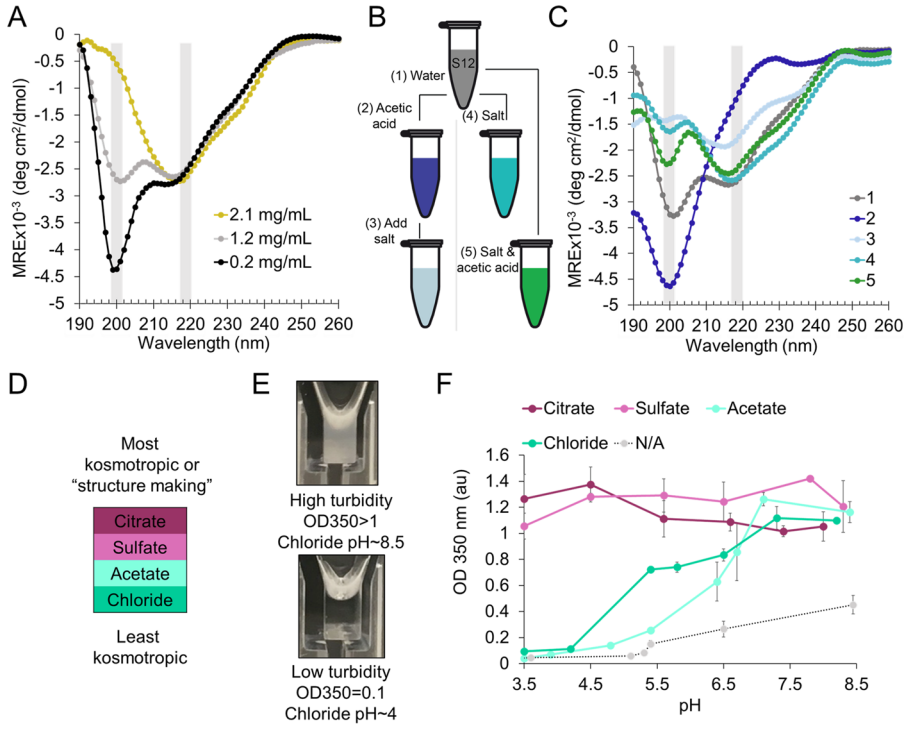

Figure 2. pH, salt, and protein concentration impact the secondary structure and solubility. (A) CD spectra of S12-pAzF at a range of protein concentrations. Gray rectangles highlight the wavelength ranges corresponding with random coil (~200 nm) and β-sheet (~217−220 nm) signatures. The mean residue ellipticity (MRE) is presented. Traces represent the average of triplicate background subtracted scans. (B) Schematic of which components were added to each sample, and the order the components were added in. Samples are color coded to correspond with (C). (C) CD spectra of S12-pAzF at 0.1 mg/mL exposed to combinations of acetic acid and/or KCl. Traces represent the average of triplicate background subtracted scans. (D) Hofmeister series ordering of the anions tested. Anions are ordered from most kosmotropic in pink shades and least kosmotropic in green shades. (E) Photographs of high (top) and low (bottom) OD 350 nm samples of S12-pAzF, showing how absorbance corresponds with turbidity in chloride salt. The concentration of protein both samples is equivalent. (F) Turbidity profiles of S12-pAzF as functions of pH and anion type. Error bars represent the standard deviation between three independent replicates.

228, and Phe 230. After purification and liquid chromatography mass spectrometry (LC−MS) analysis, we observed truncation products in all cases other than Gly 32 (Supporting Information Figure S1). Given full-length and high-level product expression, we selected the Gly 32 site to move forward with. S12-pAzF was specifically designed such that interactions impacting pH responsiveness and the secondary structure would not be interrupted. Unless otherwise noted, all studies were performed with S12-pAzF with pAzF at position 32; altering the position of pAzF incorporation could change protein behavior, and our characterizations are specific to the mutant presented here.

For the purification of S12wt and S12-pAzF, we optimized a columnless pH-cycling method[30,33] to obtain product at >90% purity (Supporting Information Figure S2). We confirmed the molecular weights of S12 and S12-pAzF using LC−MS. The deconvoluted spectra showed two major peaks in each sample: one corresponding to the theoretical masses of the full-length product and the other corresponding with the methionine-cleaved proteins (Figure 1B). Enzymatic cleavage of the N-terminal initiator methionine is a common protein modification that is regularly observed in mass spectrometry.[39] Additionally, the N-terminal protein sequence of S12-pAzF is amenable to enzymatic cleavage by *E. coli* methionine aminopeptidase.[40] We did not observe ions corresponding with truncated or misincorporation products in the S12-pAzF sample, demonstrating that small truncation products do not copurify with S12-pAzF and that pAzF-incorporation is high fidelity.[41] With S12-pAzF in hand, we tested for biorthogonal conjugation using the strain-promoted azide−alkyne cycloaddition reaction (SPAAC) with a strained alkyne dibenzocyclooctyne TAMRA fluorophore (DBCO-TAMRA) (Figure 1C).[36] Using SDS-PAGE to analyze SPAAC reaction products, we observed a uniform increase in molecular weight that was accompanied by an in-gel fluorescence signal, confirming the covalent conjugation of TAMRA to S12 (S12-TAMRA) (Figure 1D). DBCO-TAMRA did not react with S12wt, indicating that SPAAC labeling was biorthogonal and specific.

These results demonstrate several useful features of S12 and S12-pAzF. First is the ease of upstream expression and downstream purification of S12 and mutants thereof. We observed strong overexpression bands for S12, indicating that it can be produced at high yields in *E. coli* without the need for extensive optimizations (Supporting Information Figure S2). For the downstream processing of S12wt and S12-pAzF, our columnless purification protocol was readily scaled to process up to 10 L of expression culture and yielded >300 mg of purified protein per liter of culture. The yields of S12 are an order of magnitude above what has been reported for other recombinantly produced suckerins, showing promise for scalability.[33] We obtained purities of 98% and 92% for S12wt and S12-pAzF (Figure 1D), respectively, demonstrating that, while columnless purification can be more cost-effective than traditional column chromatography, the product purity is comparable. Our results also show that orthogonal translation systems (OTSs) provide an avenue for obtaining workable

https://dx.doi.org/10.1021/acssynbio.0c00442
ACS Synth. Biol. 2020, 9, 3388−3399

yields of pAzF-incorporated proteins. Of specific importance for suckerin materials and other cationic proteins, SPAAC readily proceeded under acidic conditions, providing an avenue for functionalizing proteins that are not soluble at neutral pH conditions (Supporting Information Figure S3). Thus, pAzF represents an option for expanding the chemistry of proteins when other common protein conjugation methods, like maleimide labeling on cysteine or *N*-hydroxysuccinimide ester labeling with lysine, are inaccessible due to pH constraints. It is notable that many β-sheet-rich silk fibroins are not amenable to recombinant expression; therefore, interfacing ncAA with suckerins is an attractive avenue for producing β-sheet-rich materials that can be readily and site-specifically functionalized.[30]

pH, Salt, and Protein Concentration Impact Secondary Structure and Solubility. Understanding how simple biochemical parameters like protein concentration, pH, and salt impact secondary structure is foundational to engineering NAs with new suckerin isoforms. To discover the impact of these parameters on secondary structure and β-sheet formation in S12-pAzF, we used circular dichroism (CD) spectroscopy. Since standard CD analysis software did not yield reasonable secondary structure predictions—an observation that has been made with CD analysis of other suckerin proteins—we analyzed the data qualitatively using spectral signatures that have been confirmed with Fourier-transform infrared (FTIR) spectroscopy elsewhere.[18,33] For a conservative interpretation of the CD data, we restricted the analysis to comparing spectral signatures (e.g., minima and maxima) within a given spectrum.

Previous work has shown that secondary structure, β-sheet enrichment, and the oligomerization state of suckerins are dependent on the concentration of protein in solution.[33] To characterize the impacts of protein concentration and molecular crowding on a secondary structure, we obtained the CD spectra at three concentrations: 0.2, 1.2, and 2.1 mg/mL (Figure 2A). The protein at 0.2 mg/mL exhibited both a random coil structure and β-sheet structure, indicated by minima at 195−205 and 210−220 nm, respectively. As the concentration of the protein was increased, the compositions of the β-sheet and random coil changed, with the β-sheet eventually becoming the dominant spectral feature at the highest concentration tested. Our results showing higher contributions of the random coil at higher dilution factors in S12-pAzF are in agreement with previous studies.[33] As the concentration of the protein increases, the weak interactions that promote structure, supramolecular assembly, and the formation of naturally occurring colloids—such as formation of inter- and intramolecular β-sheets and $\pi-\pi$ stacking between tyrosine residues—are more prominent than at lower concentrations.[26,33] Thus, as the solution is diluted, the propensity of these interactions to occur decreases, causing the protein to adopt a less structured and more random coil conformation.

To test the impacts of pH and salt, we exposed 0.1 mg/mL solutions of S12-pAzF to acetic acid and potassium chloride (KCl), adding these components alone, together, or sequentially (Figure 2B). The choice of 0.1 mg/mL S12-pAzF was informed by previous self-assembly studies with S19.[32] The acidification of S12-pAzF in water resulted in a conformational switch, causing the protein to adopt a predominantly random coil structure (Figure 2C). While the acidification destabilized the β-sheets, the interaction of salt ions with proteins and solvating water molecules can promote protein folding and the stabilization of a secondary structure. Upon adding KCl salt to S12-pAzF in water, it retained both the β-sheet and random coil structures (Figure 2C). When KCl and acetic acid were added simultaneously, we again observed the presence of both β-sheet and random coil structures, showing that chloride salt stabilizes β-sheets, even in pH conditions that would otherwise be destabilizing.

With the interest of controlling self-assembly, we next asked whether the β-sheet character could be restored by adding KCl after acidification and β-sheet unfolding. Indeed, introducing KCl to acidified S12-pAzF caused a chain collapse and re-emergence of β-sheets, likely *via* the charge neutralization by chloride ions on positively charged His residues (Figure 2C).[32] These results demonstrate that β-sheets in S12-pAzF can be reversibly unfolded and refolded, allowing for control of the chain collapse by manipulating solvent conditions. The process of unfolding and dispersing naturally occurring suckerin colloids using acetic acid pretreatment has been shown to be a key step for salting out suckerin NAs with narrow size distributions.[32] Importantly, the efficiency of pH-dependent β-sheet unfolding with acid is dependent on the concentration of the protein. Previous studies indicate that, as the concentration of the protein is increased, the retention of β-sheet enrichment, even in the presence of acid, is observed.[33] Thus, our secondary structure characterizations allowed us to (i) identify a protein concentration range where the secondary structure elements of S12-pAzF could be controllably unfolded and refolded (Figure 2C) and (ii) demonstrate that the protein concentration impacts the S12-pAzF secondary structure enrichment (Figure 2A).

Salt anions, which mediate the chain collapse and assembly in suckerins, have complex interactions with positively charged His side chains, the protein backbone, and with solvating water molecules.[30,42−44] Also, the choice of salt and ionic strength can impact the kinetics of protein NA assembly and, in some cases, the structure and release profile of the resulting particles.[45−47] The Hofmeister series describes some salts as kosmotropes (derived from Greek for order), characterized by a tendency to stabilize or increase the attractive interactions between hydrophobes in solution.[44] To characterize differences between four common Hofmeister series kosmotropes (Figure 2D) for salting out S12-pAzF, we employed a high-throughput spectrophotometric method where the optical density at 350 nm (OD 350 nm) was measured, noting that increases in OD are due to the assembly of higher-order structures that scatter light and increase the solution turbidity.[48,49] Figure 2E shows representative photographs of high-turbidity (OD > 1) and low-turbidity (OD = 0.1) S12-pAzF samples. Because pH impacts the solubility, secondary structure, and charge-screening effects, we tested each salt at a range of pHs.

In citrate and sulfate salts (the most kosmotropic salts), we observed high turbidity (OD > 1) over the whole pH range tested, indicating the presence of large aggregates regardless of pH and little dynamic range for tuning the particle size under these conditions (Figure 2F). In the lesser kosmotropic chloride and acetate salts, we observed a pH-dependent response and a higher dynamic range for tuning the assembly state of S12-pAzF using pH. Specifically, below pH 4.5, the turbidity remained low (OD < 0.2), indicating conditions for fabricating nanoscale assembles or a lack of assembly. Above pH 4.5 but below the pK_a of the imidazole side chain of His ($pK_a \sim 6$), we observed significant increases in OD, indicating

https://dx.doi.org/10.1021/acssynbio.0c00442
ACS Synth. Biol. 2020, 9, 3388−3399

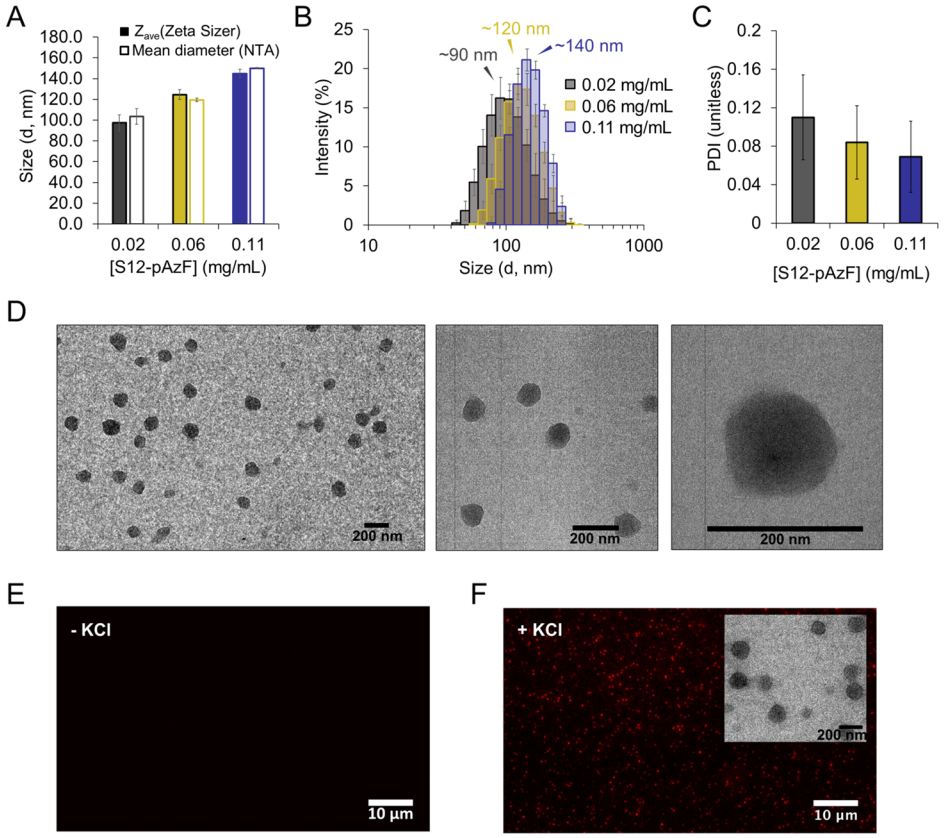

Figure 3. Salting out and functionalizing S12-pAzF NAs. (A) DLS analysis of S12-pAzF NAs fabricated at three concentrations of S12-pAzF. Solid bars show the average diameter (Z_{ave}) measured by a Zeta Sizer, and outlined bars show the mean diameter measured *via* nanoparticle tracking analysis (NTA). Error bars represent the standard deviation between measurements of three independently prepared batches of NAs. (B) Particle size distributions of S12-pAzF NAs. Annotations indicate the size corresponding with the approximate intensity maximum measured in each sample. Error bars represent the standard deviation between three independently prepared batches of NAs. (C) Polydispersity indices of NAs measured by a Zeta Sizer. Error bars represent the standard deviation between three independently prepared batches of NAs. (D) Representative TEM micrographs of NAs fabricated at 0.11 mg/mL S12-pAzF, with magnification increasing from left to right. (E) Fluorescence microscopy image of S12-TAMRA with no salt added. (F) Fluorescence microscopy image of S12-TAMRA with KCl added to salt out NAs. The inset shows a TEM micrograph of the corresponding fluorescent S12-TAMRA NAs. Data are representative of three independent experiments.

assembly *via* charge screening on His residues (Figure 2F). As the pH approached 7, a high turbidity was observed in all samples, indicating that the deprotonation of His residues results in unconstrained aggregation with or without salt. Notably, these trends were observed in both sodium and potassium salts, providing evidence that anion-mediated effects dominate the observed behavior (Supporting Information Figure S4).

These results show that S12-pAzF salting out follows the direct Hofmeister series, with the most kosmotropic salts precipitating S12-pAzF most efficiently over the conditions tested. This corroborates our previous observations that the chain collapse in cross-linked S12 hydrogels was mediated by anions and that the kinetics of hydrogel contraction trended with the kosmotropic arm of the Hofmeister anion series.[30] We postulate that differences in pH response across salts is due to (i) differences in anion avidity for charged His residues and (ii) the mediation of interactions with other parts of the protein (such as hydrophobic patches in amorphous domains) by the more kosmotropic salts. Future studies using quantitative methods to discern structure and protein/solvent interactions, such as FTIR or nuclear magnetic resonance spectroscopy, could be used to elucidate the mechanisms behind the observed behavior. Additionally, the use of molecular dynamics has already been employed to study the structure of minimal suckerin peptides and could be applied to understand in greater depth the molecular mechanisms behind our findings.[26,50] Since the salt identity has previously been used to tune NA size using S19, these results show which salts are potentially useful for engineering pH-dependent self-assembly processes with S12-pAzF and provide information about the impact of salt identity on self-assembly.

Salting out and Functionalizing S12-pAzF NAs. With an understanding of the process variables impacting the β-sheet enrichment and solubility of S12, we sought to characterize S12-pAzF NAs salted out with a chloride salt. In initial optimizations, we used dynamic light scattering (DLS) to characterize influences of protein concentration, acidification, and salt concentration on particle size distributions. Supporting Information Figure S5 shows an average diameter (Z_{ave}), polydispersity index (PDI), and transmission electron microscopy (TEM) characterization of select conditions. Particle size distributions (PSDs) are presented in Supporting Information Figure S6. We observed several trends from these experiments. The factor that contributed most significantly to constraining particle sizes was acidification prior to the addition of KCl. These conditions resulted in the formation of discrete NAs with narrow size distributions (Supporting

https://dx.doi.org/10.1021/acssynbio.0c00442
ACS Synth. Biol. 2020, 9, 3388−3399

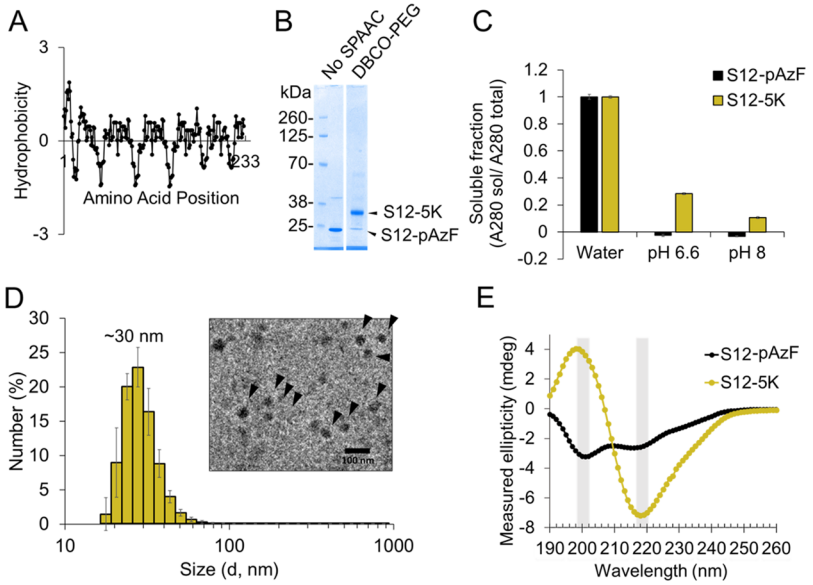

Figure 4. PEGylation of S12 changes assembly properties. (A) Kyte and Doolittle hydrophobicity plot of S12. Residues corresponding with positive values are hydrophobic. Plot was generated using the ProtScale (ExPASy) using a window size of 9 and a linear weight variation model. (B) SDS-PAGE analysis of S12-5K, showing conjugation of 5 kDa PEG to S12-pAzF *via* SPAAC. Unconjugated S12-pAzF and the S12-5K conjugation product are indicated. Uncropped gel is shown in Supporting Information Figure S8. (C) Soluble (sol) fraction S12-pAzF and S12-5K in water, MES pH 6.6, and Tris pH 8. Error bars represent the standard deviation of three independently prepared samples. (D) DLS analysis of S12-5K in water. The inset shows an electron micrograph of S12-5K particles, with black arrows indicating particles for clarity. Error bars represent the standard deviation of three independently prepared samples. (E) CD analysis of S12-pAzF and S12-5K in water. Gray rectangles highlight the wavelength ranges corresponding with random coil (~200 nm) and β-sheet (~217−220 nm) signatures. Traces represent the average of triplicate background subtracted scans.

Information Figures S5 and S6). When the solvent was not acidified, we observed relatively large average particle diameters, higher PDIs, and the formation of micron-scale, irregularly shaped aggregates of particles upon the addition of KCl (Supporting Information Figure S5). We also observed that decreasing the protein concentration and lowering the process temperature decreased average particle sizes, suggesting that controlling the kinetics of aggregation constrains particle diameters.

Guided by our optimizations, we identified conditions for fabricating ~100 nm particles, since this is a desirable size regime for biomedical applications. We preacidified S12-pAzF and then salted out NAs fabricated at three concentrations of protein using 250 mM KCl. Here, we observed that average particle sizes increased as the protein concentration was increased. We confirmed the rank-order of average particle sizes using two in-solution dynamic light scattering (DLS) techniques: a bulk measurement using a Zeta Sizer and nanoparticle tracking analysis (NTA), a technique that individually tracks and sizes particles in a flowcell over time. Specifically, for particles fabricated at 0.02, 0.06, and 0.11 mg/mL of S12-pAzF, particle sizes were ~100, ~ 120, and 150 nm, respectively, with particle sizes increasing with the protein concentration (Figure 3A). PSDs and PDIs measured *via* a Zeta Sizer are shown in Figure 3B,C, and the associated NTA PSDs are presented in Supporting Information Figure S7. PDI, a metric of the broadness of the measured size distribution that was calculated directly from the DLS correlation data, was low (<0.15) for each condition, showing uniform particle sizes. TEM images are shown for the 0.11 mg/mL condition in Figure 3D, confirming the presence of circular ~150 nm particles, consistent with scattering data. Images for the 0.02 and 0.06 mg/mL conditions are presented in Supporting Information Figure S7.

Salting out suckerin NAs *via* β-sheet formation is hypothesized to be a kinetic process where decreasing the temperature and protein concentration decreases the particle size.[32] Since the particles fabricated at the three concentrations of protein have similar morphologies and relatively low PDIs, we hypothesize that, in each case, self-assembled particles are formed due to induction of β-sheet formation with the addition of KCl. It is notable here that analogous self-assembly processes with β-sheet-rich silk fibroins have also revealed decreasing particle size with decreasing protein concentration.[45,51] Additionally, our observations of changes in particle size with the concentration of protein is a commonly observed phenomenon in the self-assembly of block copolymer systems.[52] The morphologies of NAs indicated that the particles were protein-core, as opposed to hollow-core or micellar. This morphology is similar to what has been observed with functional S19 NAs.[32] The methods used here to salt out S12-pAzF NAs are similar to those used previously for S19 NAs, indicating that the experimental techniques used here could be generalizable for characterizing the self-assembly of other suckerins, both natural and synthetic.

Previous efforts for preparing functional self-assembled suckerin NAs involved the sequestration of hydrophobic drug cargo through noncovalent interactions.[32] Noncovalent loading methods, however, suffer from a lack of control of the loading density and release of cargo. The covalent conjugation of cargo offers an improved level of control for fabricating drug-loaded therapeutic nanocarriers and fine-tuning release profiles.[53−56] Toward this eventual goal, we fabricated particles using S12-TAMRA, since the TAMRA fluorophore is a hydrophobic molecule. Using fluorescence microscopy, we

https://dx.doi.org/10.1021/acssynbio.0c00442
ACS Synth. Biol. 2020, 9, 3388−3399

observed the formation of dispersed, circular particles only upon the addition of KCl (Figures 3E,F). The morphology and size of TAMRA-conjugated NAs were similar to those of NAs fabricated without a fluorophore, showing that self-assembly proceeds similarly with a conjugate small molecule (Figure 3F, inset). Since the relatively small size of the conjugated fluorophore (0.9 kDa) allowed self-assembly to proceed unhindered, we hypothesize that small molecules of similar sizes and hydrophobicities to TAMRA, like small-molecule cancer therapeutics, could likely be loaded into S12-derived NAs using the same approach. These results pave the way for future studies to fabricate precisely defined and drug-loaded NAs. Since multiple installations of pAzF (>30) within a single protein are accessible with the OTS used here, future studies could also interrogate the feasibility of higher small-molecule loading densities.[41,57]

PEGylation of S12-pAzF Changes Assembly Properties. We next sought to leverage site-specific functionalization to rapidly build and test conjugates of S12-pAzF with altered hydrophobicity. Altering the compositions of hydrophobic/hydrophilic sequences in polymers is a strategy for engineering the self-assembly and crystallinity of block copolymers.[22,58−65] For proteins, this process can often involve tedious cloning procedures (since highly repetitive DNA sequences are challenging to synthesize), and the protein expression of many variants can be daunting.[66] Thus, the ability to use SPAAC to controllably functionalize proteins with hydrophilic ligands could expedite designing and building synthetic amphiphiles and could eventually guide the design of engineered protein sequences with precisely defined properties.

The amino acid sequence of S12 is mostly hydrophobic (Figure 4A), and the hydrophobic interactions of inter- and intramolecular β-sheets are critical for S12 self-assembly. Thus, we reasoned that covalently conjugating a model hydrophilic polymer, polyethylene glycol (PEG), to S12-pAzF would alter protein properties. Using SPAAC, we conjugated S12-pAzF to a 5 kDa PEG (referred to as S12-5K) molecule with >90% efficiency, as determined by densitometry analysis of Coomassie-stained SDS-PAGE gels (Figure 4B). We tested for changes in the solubility between S12-pAzF and S12-5K in water and in two buffer/pH combinations where the unconjugated protein is insoluble: MES buffer at pH 6.6 and Tris buffer at pH 8. PEGylation improved the solubility of S12-pAzF, by 28% and 11% at pH 6.6 and pH 8, respectively, showing that increasing the hydrophilicity of S12 improves the solubility at near or above physiological pH (Figure 4C). S12-5K formed circular particles on the order of 30−50 nm in size in water, where unconjugated S12-pAzF did not exhibit a measurable particle formation or stable DLS spectra (Figure 4D). Increasing the molecular weight of the PEG molecule to 10K changed the properties further, increasing the solubility of the conjugate to >75% at pH > 6 and changing the morphology to a soluble fibrillar network of particles (Supporting Information Figure S8).

To better understand the impacts of PEGylation on S12-pAzF properties, we studied the secondary structure of S12-5K. Despite its increased hydrophilicity, S12-5K displayed a significant enrichment in the β-sheet character compared with S12-pAzF, potentially increasing its propensity to self-assemble. The CD spectra of both S12-pAzF and S12-5K displayed a broad minimum near 210−220 nm (indicating β-sheet character), with the minimum being more pronounced for S12-5K (Figure 4E). However, where S12-pAzF displayed a minimum at 200−210 nm, indicative of a random coil, the S12-5K spectrum displayed a switch to positive ellipticity with a peak between 200 and 210 nm (Figure 4E). These spectral features indicate a significant decrease in the random coil signature and an enrichment of β-sheet content in S12-5K. Taken together, our results indicate that PEGylation, while increasing the solubility of S12 by increasing hydrophilicity, also induced changes in β-sheet content, orientation, and presentation in S12-5K. Since β-sheet formation is a driving force for molecular self-assembly, the modulation of β-sheet content and therefore PEGylation changes the propensity for inter- and intraprotein hydrophobic interactions. While further studies are needed to understand the impact of PEG length on the secondary structure and emergent properties, our results demonstrate that the alteration of S12-pAzF using PEGylation *via* SPAAC can result in conjugates that have altered solubility and assembly properties.

CONCLUSION

Here, we characterized the salt and pH responsiveness of suckerin-12, a promising protein for fabricating functional NAs. We optimized self-assembly and identified conditions for fabricating ∼100 nm suckerin-based NAs using a simple salting-out procedure. We anticipate that our workflow will be a useful framework for future efforts in fabricating and processing natural and synthetic suckerin materials. Finally, we showed that the ncAA pAzF is useful for obtaining high yields of recombinant S12-pAzF, which can be efficiently functionalized using SPAAC. The ability to site-specifically modify S12 allowed us to fabricate ∼100 nm fluorophore-loaded NAs and to alter the assembly properties of S12. In future studies, the S12-pAzF scaffold described here could be used to make functional materials such as NAs with precise drug loading or self-assembling amphiphiles, where functional hydrophilic molecules other than PEG (such as DNA or carbohydrates) are used to impact the assembly and enhance functionality. Ultimately, we anticipate that ncAAs will expedite the development of functional nanomaterials by allowing researchers to quickly synthesize new protein conjugates with desired properties.

MATERIALS AND METHODS

Expression of S12wt and S12-pAzF. The open reading frame of S12 was obtained from Uniprot (Identifier # A0A075LXT7_DOSGI) and synthesized by Integrated DNA technologies without the signal peptide. The gblock was cloned into the IPTG-inducible pET28a (Novagen) to make the expression plasmid pET28a-S12. For S12-pAzF, the codon encoding glycine 32 was mutated to the amber stop codon (TAG) *via* PCR mutagenesis, resulting in the pET28a-S12-TAG expression vector. For S12wt, pET28a-S12 was transformed into BL21 Star (DE3), selected on LB agar plates supplemented with 50 ug/mL Kanamycin, and grown overnight at 37 °C. For S12-pAzF, pET28a-S12-TAG was cotransformed with the arabinose-inducible pEVOL-pAzFRS.2.t1 (Addgene, Plasmid #73546) and selection plates contained 50 μg/mL Kanamycin and 34 μg/mL Chloramphenicol. Cells were always freshly transformed. For expression, single colonies were selected and grown overnight at 37 °C in 2xYTP media supplemented with appropriate antibiotic(s). Expression cultures were grown in shake flasks (1 L scale) or a Sartorius Stedim BIOSTAT Cplus bioreactor (10 L scale) at

https://dx.doi.org/10.1021/acssynbio.0c00442
ACS Synth. Biol. 2020, 9, 3388−3399

37 °C with antibiotics. S12 expression was induced during exponential growth at OD 0.6−0.8 with 0.5 mM IPTG. For S12-pAzF expression, cultures were supplemented with 0.5 mM IPTG, 0.1% (w/v) arabinose, and 3 mM pAzF (Chem-Implex Int'l Inc.) at induction. The expression proceeded overnight at 30 °C. Expression cultures were harvested at 5000*g* for 15 min at room temperature. Cells were washed once with Buffer 1 (50 mM Tris, pH 8, and 100 mM NaCl), flash frozen with liquid nitrogen, and stored at −20 °C until purification.

Inclusion Body Purification of S12 and S12-pAzF. For purification, we adapted an inclusion body preparation from Buck and colleagues.[30] Unless otherwise noted, all steps were performed at room temperature. The cell pellets were thawed and resuspended in 30 mL of Buffer 1 per 0.5 L of expression culture. Lysozyme was added to the resuspended cells to a final concentration of 1 mg/mL and incubated for 30 min. The cells were sonicated on ice using a Q125 Sonicator (Qsonica, Newtown) with a 3.175 mm diameter probe at a frequency of 20 kHz and 45% amplitude. Energy was delivered to cells in pulses of 15 s, followed by 15 s off, for 10 min total. Lysed cells were centrifuged at 10 000*g* for 10 min. The supernatant containing soluble cellular proteins was discarded, and inclusion bodies containing S12 were collected in the pellet. Pellets were resuspended for washing in 35 mL of Buffer 1 supplemented with 1% Triton X-100 (v/v) by light vortexing. After dispersion, suspensions were incubated on an orbital shaker for 10 min at 4 °C. Pellets were collected by centrifugation at 5000*g* for 15 min. Washes with Triton X-100 supplemented buffer were repeated for three total washes. After washing, pellets were resuspended in 15 mL of deionized water per 1 L of expression culture, and pellets were dispersed by light vortexing and sonication. For "pH-cycling", the S12 suspension was poured into a clean beaker with stirring and pH monitoring. HCl was used to adjust the solution pH to 3 to solubilize S12. Soluble S12 was incubated for 1 h at room temperature with constant agitation and then clarified at 20 000*g* for 10 min. To precipitate S12, 1 M NaCl was mixed with the supernatant to 100 mM. Under agitation, the pH was adjusted to 8 with 1 M Tris pH 8. Insoluble S12 was recovered by centrifugation at 10 000*g* for 10 min. Another round of solubilization and precipitation was conducted to improve the purity. Pellets were resuspended to ∼5 mg/mL of S12 in 5% (v/v) acetic acid and dialyzed exhaustively against water using 20 000 MWCO membranes (ThermoFisher Scientific). No specific procedures were performed for refolding. For quantitation of the protein concentration, the sample absorbance at 280 nm was measured using a Nanodrop 2000 (Thermo Scientific). The molar extinction coefficient and molecular weight of S12 were used to calculate the protein concentration. S12wt and S12-pAzF were aliquoted, flash frozen on liquid nitrogen, and stored at ∼6 mg/mL at −80 °C until use. Expression yields of S12wt and S12-pAzF were calculated using the following formula:

$$\frac{[\mathrm{S12}] \times V_{\mathrm{S12}}}{V_{\mathrm{culture}}} \quad (1)$$

where [S12] is the concentration of S12 measured in the purified product in milligrams per milliliter, V_{S12} is the volume of purified S12 in milliliters, and V_{culture} is the volume of *E. coli* culture used for recombinant production in liters.

Strain-Promoted Azide−Alkyne Cycloaddition (SPAAC) Reactions. S12-pAzF was labeled using strain-promoted azide−alkyne cycloaddition (SPAAC) using various dibenzocyclooctyne (DBCO) probes. SPAAC reactions were conducted in water (unless otherwise noted) at 0.02 mM S12-pAzF incubated with 2 mM strained alkyne probes. Reactions were incubated overnight at 30 °C in an end-over-end mixer with constant rotation, followed by exhaustive dialysis into water using 20 000 MWCO membranes (Thermo Fisher Scientific). To make stock solutions, DBCO-TAMRA (Millipore Sigma) was resuspended to 10 mM in 100% DMSO and DBCO-mPEG 5 kDa/DBCO-mPEG 10 kDa (Broad Pharm) was resuspended to 10 mM in water. All DBCO probe stocks were stored at −20 °C. The labeling efficiency was determined using SDS-PAGE, followed by densitometry analysis and in-gel fluorescence.

Turbidity Profiles. The salt response of S12-pAzF was investigated using turbidity profiles. All salts were purchased from Sigma. The solutions of the following salts were prepared at 500 mM: potassium acetate, sodium acetate, potassium chloride, sodium chloride, potassium sulfate, sodium sulfate, potassium citrate, and sodium citrate. After dissolving, the salts were brought to the desired pH using glacial acetic acid (regardless of the salt anion), NaOH for sodium salts, and KOH for potassium salts. Twenty microliters of S12-pAzF at 0.5 mg/mL in water was pipetted into the wells of a black Costar 384 well plate with a clear bottom for imaging (Corning). Twenty microliters of salt solutions was added to each well to 250 mM salt (40 μL total volume) and mixed well. The plates were quickly spun down to remove bubbles and then sealed and equilibrated for 1 h at room temperature on an orbital shaker. After incubation, the optical density at 350 nm (OD 350) and pH were measured using a Synergy H1 microplate reader (Biotek) and an Orion pH probe (Millipore Sigma), respectively. OD 350 of triplicate wells for each condition were averaged and background subtracted by the average OD 350 of triplicate wells containing 40 μL of pH-adjusted salt at 250 mM with no protein.

Salting-out S12 NAs. A fresh aliquot of S12-pAzF was thawed on ice and diluted to 2× the final desired concentration in ice-cold 5% (v/v) acetic acid. To disperse naturally occurring S12 colloids, the protein was sonicated for 20 min in a cold water bath and then sterile filtered using a 0.1 μm filter (Millex-VV Syringe Filter, Merck Millipore Ltd.). The resulting mixture was spun at 15 000*g* for 10 min at 4 °C; the supernatant of this spin was the working stock of protein and was prepared fresh for each experiment. For salting-out NAs, a cold KCl solution at 500 mM was quickly mixed 1:1 with the working protein stock and vigorously pipet mixed on ice. Final concentrations of KCl and acetic acid were 250 mM and 2.5% (v/v), respectively, unless otherwise noted. Notably, for initial optimization experiments (Supporting Information Figures S4 and S5), all the steps were the same as those described above, except that particles and reagents were equilibrated to room temperature before salting out and the concentrations of protein, KCl, and acetic acid were varied as indicated.

Fluorescence Microscopy. Fluorescent NAs fabricated using the TAMRA-conjugated S12 scaffold (S12-TAMRA) were observed using fluorescence microscopy. To make TAMRA-loaded S12 NAs, S12-TAMRA at 0.22 mg/mL in 5% (v/v) acetic acid was mixed 1:1 with 500 mM KCl and pipet mixed vigorously on ice. Two microliters of the sample was mounted on a glass slide for fluorescence microscopy.

https://dx.doi.org/10.1021/acssynbio.0c00442
ACS Synth. Biol. 2020, 9, 3388−3399

Particles were viewed using a Nikon Ni-U upright microscope with a 100 × 1.45 n.a. plan apochromat objective. Images were captured using an Andor Clara-Lite digital camera (Andor Technology) and Nikon NIS Elements software (Nikon Instruments Inc.). Fluorescence images were collected using a yellow excitation Y-2E/C filter combination.

SDS PAGE and in-Gel Fluorescence Assays. SDS-PAGE was run using NuPAGE 4%−12% Bis-Tris protein gels with MOPS-SDS buffer (Thermo Fisher Scientific) and either the Chameleon 800 or Chameleon Duo protein standards (LI-COR Biosciences). For total protein imaging, the gels were stained using SimplyBlue SafeStain Coomassie (Thermo Fisher Scientific) and imaged using a Gel Doc XR (Bio-Rad). Densitometry analysis for purity was conducted using ImageJ. For in-gel fluorescence assays, gels were imaged using a LI-COR Odyssey Fc (LI-COR Biosciences).

Determination of Protein Solubility. To assess changes in the solubility parameters of S12-PEG conjugates against unconjugated S12-pAzF, we exposed 1 mg/mL PEGylated or unconjugated S12-pAzF to 50 mM Tris pH 8 and 50 mM MES pH 6.6. Triplicate samples were incubated for 5 min and then clarified at 20 000*g* for 10 min. The absorbance at 280 nm (A280) of the supernatant was then measured, and the soluble fraction was calculated.

Liquid Chromatography Mass Spectrometry. Purified proteins (10 pmol, or 10 μL of 1 μM sample, each) were separated with an XBridge BEH C4 analytical column (300 Å, 3.5 mm, 2.1 mm × 50 mm, SKU 186004498; Waters) fitted with a matched guard column (2.1 mm × 10 mm, SKU 186007230; Waters) using an Agilent 1200 HPLC system and analyzed with an Agilent 6210A time-of-flight mass spectrometer equipped with an ESI source (Agilent). The aqueous phase (A) was 95% water and 5% acetonitrile with 0.1% formic acid, and the organic phase (B) was 100% acetonitrile with 0.1% formic acid. The method run at a constant 0.4 mL/min was, in brief, diversion to waste at 15.8% B for 1 min, elution into source with a 12 min gradient from 15.8% to 65.8% B, column wash with a 2 min gradient from 65.8% to 69.9% B and then 2 min at 100%, and column equilibration for 6 min at 15.8% B. TOF-MS spectra were processed using an Agilent Mass Hunter (vB.04.00). The maximum entropy method was used to deconvolute spectra for m/z = 700−2000. Deconvoluted spectra were manually analyzed for the presence/absence and relative abundances of the following species on the basis of theoretical molecular weights: full length protein with pAzF (TAG construct) or without (wild-type construct); truncations at TAG codon; pAzF substitution with tyrosine or glycine; any protein sequence ± initiator methionine; and additional contaminants.

Circular Dichroism (CD). CD spectra were collected in triplicate scans at 25 °C using a Jasco J-810 spectrometer using the following parameters: wavelength range of 190−260 nm, scan rate of 50 nm/min, and a bandwidth of 1 nm. Triplicate scans were conducted as technical replicates.[27,33] The background absorbance from each buffer/path length combination was measured before acquiring the spectra and automatically subtracted by the CDPro software during acquisition (Jasco). The spectra were averaged and smoothed using the Savitzky−Golay method using CDPro. Traces were converted to a mean residue ellipticity (MRE) where appropriate. For CD measurements where pH and salt content were varied, 0.5% (v/v) acetic acid and/or 50 mM KCl was used. For CD measurements comparing PEGylated S12 (S12-5K) and unconjugated S12-pAzF, measurements were conducted with 0.1 mg/mL S12-pAzF or S12-5K in water.

Dynamic Light Scattering (DLS) Measurements. DLS measurements were performed on a Malvern Zetasizer Nano ZS with a measurement angle of 173° in disposable cuvettes with a sample volume of 70 μL (Malvern Panalytical). All measurements were collected in triplicate for 13 scans per measurement. The refractive index and viscosity were obtained from the instrument's parameter library. The instrument's "General Purpose" setting was used to calculate particle size distributions (PSDs). Samples were analyzed directly without dilution.

Nanoparticle tracking analysis measurements were performed on a Malvern Nanosight NS300 using a 642 nm red laser (Malvern Panalytical). Samples were diluted directly before analysis to manufacturer-recommended particle concentrations in sterile 250 mM KCl, 2.5% acetic acid. Samples were flowed into the cell, and the instrument was focused according to the manufacturer recommendations. Measurements were collected at room temperature, using a 1 mL syringe and a syringe pump infusion rate of 40 (arbitrary units). Data for each sample was collected in three separate 1 min videos, under continuous flow conditions. Mean particle diameters and PSDs were obtained from aggregate Nanosight experiment reports of each run and then averaged across triplicates and corrected for the dilution factor. For PSDs, curves were normalized before plotting.

Transmission Electron Microscopy (TEM). NAs were visualized by TEM. For TEM measurement, 200 mesh Cu grids with a Formvar/Silicon Monoxide (Cat #1830, Ted Pella Inc.) were placed in a Pelco easiGlow glow discharger (Ted Pella Inc.) and an atmosphere plasma was introduced on the surface of the grids for 30 s with a current of 15 mA at a pressure of 0.24 mbar. This treatment creates a negative charge on the carbon membrane, allowing for liquid samples to spread evenly over the grid. Four microliters of sample was pipetted onto the grid and incubated for 2 min before wicking excess liquid from the grids. Grids were immediately washed with water, dried, and imaged. Notably, a stain was not used due to sample aggregation upon staining. Samples were viewed using a Hitachi HT7700 (Hitachi, Ltd.) at 80 keV. The image data was collected by a Gatan Orius SC1000A CCD camera (Gatan Inc.). The image analysis was done with ImageJ.

■ ASSOCIATED CONTENT

Supporting Information

The Supporting Information is available free of charge at https://pubs.acs.org/doi/10.1021/acssynbio.0c00442.

Figures of deconvoluted LC−MS spectra, well key of SDS-PAGE gel, SDS-PAGE analysis, precipitated and solubilized S12 from inclusion bodies photographs, in-gel fluorescence images, turbidity measurements of S12-pAzF in sodium and potassium salts of various anions, average diameters of S12- pAzF particles, associated polydispersity indexes, TEM images, intensity and number particle size distributions, and soluble fractions and methods for Cryo-TEM and expression of S12 variants for determining a pAzF mutation position (PDF)

https://dx.doi.org/10.1021/acssynbio.0c00442
ACS Synth. Biol. 2020, 9, 3388−3399

AUTHOR INFORMATION

Corresponding Author

Michael C. Jewett − *Department of Chemical and Biological Engineering, Chemistry of Life Processes Institute, Center for Synthetic Biology, Robert H. Lurie Comprehensive Cancer Center, and Simpson Querrey Institute, Northwestern University, Evanston, Illinois 60208−3120, United States;* orcid.org/0000-0003-2948-6211; Phone: +1 847-467-5007; Email: m-jewett@northwestern.edu

Authors

Jasmine M. Hershewe − *Department of Chemical and Biological Engineering, Chemistry of Life Processes Institute, and Center for Synthetic Biology, Northwestern University, Evanston, Illinois 60208−3120, United States;* orcid.org/0000-0003-4795-9721

William D. Wiseman − *Chemistry of Life Processes Institute, Center for Synthetic Biology, and Master of Biotechnology Program, Technological Institute, Northwestern University, Evanston, Illinois 60208−3120, United States*

James E. Kath − *Department of Chemical and Biological Engineering, Chemistry of Life Processes Institute, and Center for Synthetic Biology, Northwestern University, Evanston, Illinois 60208−3120, United States;* orcid.org/0000-0003-3767-9822

Chelsea C. Buck − *Materials and Manufacturing Directorate, Air Force Research Laboratory, Wright-Patterson Air Force Base, Dayton, Ohio 45433, United States; Chemical and Materials Engineering Department, University of Dayton, Dayton, Ohio 45469, United States*

Maneesh K. Gupta − *Materials and Manufacturing Directorate, Air Force Research Laboratory, Wright-Patterson Air Force Base, Dayton, Ohio 45433, United States;* orcid.org/0000-0001-8378-6595

Patrick B. Dennis − *Materials and Manufacturing Directorate, Air Force Research Laboratory, Wright-Patterson Air Force Base, Dayton, Ohio 45433, United States*

Rajesh R. Naik − *711th Human Performance Wing, Air Force Research Laboratory, Wright-Patterson Air Force Base, Dayton, Ohio 45433, United States;* orcid.org/0000-0002-7677-928X

Complete contact information is available at: https://pubs.acs.org/10.1021/acssynbio.0c00442

Author Contributions

The manuscript was written through contributions of all authors. All authors have given approval to the final version of the manuscript.

Notes

The authors declare no competing financial interest.

ACKNOWLEDGMENTS

The authors would like to thank the Center of Excellence for Bioprogrammable Nanomaterials (C-ABN) through the Air Force Research Laboratories for providing funding (FA8650-15-2-5518) and a collaborative infrastructure for our research. This work made use of the EPIC, Keck-II, IMSERC, and facilities of Northwestern University's NUANCE Center, which have received support from the Soft and Hybrid Nanotechnology Experimental (SHyNE) Resource (NSF NNCI-1542205), the MRSEC program (NSF DMR-1121262) at the Materials Research Center, the International Institute for Nanotechnology (IIN), the Keck Foundation, and the State of Illinois, through the IIN. The authors would like to thank Miles Markmann and Eric Roth for helpful conversations about TEM. The authors would like to thank Marquise Crosby for helpful conversations about protein purification. J.M.H. was supported by the National Defense Science and Engineering Graduate Fellowship, the C-ABN, and the Ryan Fellowship. M.C.J. acknowledges the David and Lucile Packard Foundation and the Camille Dreyfus Teacher-Scholar Program for support. P.B.D. is adjunct faculty at Wright State University, Dayton, Ohio. R.R.N. acknowledges funding support from AFOSR.

ABBREVIATIONS

CD, circular dichroism; DBCO, dibenzocyclooctyne; DLS, dynamic light scattering; FTIR, Fourier-transform infrared; LC−MS, liquid chromatography mass spectrometry; MRE, mean residue ellipticity; NA, nanoassemblies; ncAA, non-canonical amino acids; NTA, nanoparticle tracking analysis; OD, optical density; OTS, orthogonal translation system; pAzF, para-*L*-azido-phenylalanine; PDI, polydispersity index; PEG, polyethylene glycol; PSD, particle size distribution; S12, suckerin-12; S19, suckerin-19; SPAAC, strain-promoted azide−alkyne cycloaddition; SRT, sucker ring teeth; TEM, transmission electron microscopy

REFERENCES

(1) Martin, J. D., Cabral, H., Stylianopoulos, T., and Jain, R. K. (2020) Improving cancer immunotherapy using nanomedicines: progress, opportunities and challenges. *Nat. Rev. Clin. Oncol. 17*, 251−266.

(2) van der Meel, R., Sulheim, E., Shi, Y., Kiessling, F., Mulder, W. J. M., and Lammers, T. (2019) Smart cancer nanomedicine. *Nat. Nanotechnol. 14*, 1007−1017.

(3) Caster, J. M., Patel, A. N., Zhang, T., and Wang, A. (2017) Investigational nanomedicines in 2016: a review of nanotherapeutics currently undergoing clinical trials. *Wiley Interdiscip. Rev. Nanomedicine Nanobiotechnology. 9*, No. e1416.

(4) Webber, M. J., Appel, E. A., Meijer, E. W., and Langer, R. (2016) Supramolecular biomaterials. *Nat. Mater. 15*, 13−26.

(5) Numata, K. (2020) How to define and study structural proteins as biopolymer materials. *Polym. J. 52*, 1043−1056.

(6) Maskarinec, S. A., and Tirrell, D. A. (2005) Protein engineering approaches to biomaterials design. *Curr. Opin. Biotechnol. 16*, 422−426.

(7) Smits, F. C. M., Buddingh, B. C., Van Eldijk, M. B., and Van Hest, J. C. M. (2015) Elastin-like polypeptide based nanoparticles: Design rationale toward nanomedicine. *Macromol. Biosci. 15*, 36−51.

(8) MaHam, A., Tang, Z., Wu, H., Wang, J., and Lin, Y. (2009) Protein-based nanomedicine platforms for drug delivery. *Small 5*, 1706−1721.

(9) Spiess, K., Lammel, A., and Scheibel, T. (2010) Recombinant spider silk proteins for applications in biomaterials. *Macromol. Biosci. 10*, 998−1007.

(10) Despanie, J., Dhandhukia, J. P., Hamm-Alvarez, S. F., and MacKay, J. A. (2016) Elastin-like polypeptides: Therapeutic applications for an emerging class of nanomedicines. *J. Controlled Release 240*, 93−108.

(11) Hiew, S. H., and Miserez, A. (2017) Squid Sucker Ring Teeth: Multiscale Structure-Property Relationships, Sequencing, and Protein Engineering of a Thermoplastic Biopolymer. *ACS Biomater. Sci. Eng. 3*, 680−693.

(12) Miserez, A., Weaver, J. C., and Chaudhuri, O. (2015) Biological materials and molecular biomimetics - filling up the empty soft materials space for tissue engineering applications. *J. Mater. Chem. B 3*, 13−24.

(13) Guerette, P. A., Hoon, S., Seow, Y., Raida, M., Masic, A., Wong, F. T., Ho, V. H. B., Kong, K. W., Demirel, M. C., Pena-Francesch, A., Amini, S., Tay, G. Z., Ding, D., and Miserez, A. (2013) Accelerating the design of biomimetic materials by integrating RNA-seq with proteomics and materials science. *Nat. Biotechnol. 31*, 908−15.
(14) Sariola, V., Pena-Francesch, A., Jung, H., Çetinkaya, M., Pacheco, C., Sitti, M., and Demirel, M. C. (2015) Segmented molecular design of self-healing proteinaceous materials. *Sci. Rep. 5*, 13482.
(15) Pena-Francesch, A., Jung, H., Demirel, M. C., and Sitti, M. (2020) Biosynthetic self-healing materials for soft machines. *Nat. Mater. 19*, 1230.
(16) Costa, S. A., Simon, J. R., Amiram, M., Tang, L., Zauscher, S., Brustad, E. M., Isaacs, F. J., and Chilkoti, A. (2018) Photo-Crosslinkable Unnatural Amino Acids Enable Facile Synthesis of Thermoresponsive Nano- to Microgels of Intrinsically Disordered Polypeptides. *Adv. Mater. 30*, 1704878.
(17) Arranz-Gibert, P., Vanderschuren, K., and Isaacs, F. J. (2018) Next-generation genetic code expansion. *Curr. Opin. Chem. Biol. 46*, 203−211.
(18) Deepankumar, K., Lim, C., Polte, I., Zappone, B., Labate, C., De Santo, M. P., Mohanram, H., Palaniappan, A., Hwang, D. S., and Miserez, A. (2020) Supramolecular β-Sheet Suckerin-Based Underwater Adhesives. *Adv. Funct. Mater. 30*, 1907534.
(19) Sengupta, D., and Heilshorn, S. C. (2010) Protein-engineered biomaterials: highly tunable tissue engineering scaffolds. *Tissue Eng., Part B 16*, 285−293.
(20) Carrico, I. S., Maskarinec, S. A., Heilshorn, S. C., Mock, M. L., Liu, J. C., Nowatzki, P. J., Franck, C., Ravichandran, G., and Tirrell, D. A. (2007) Lithographic patterning of photoreactive cell-adhesive proteins. *J. Am. Chem. Soc. 129*, 4874−4875.
(21) Link, A. J., Mock, M. L., and Tirrell, D. A. (2003) Non-canonical amino acids in protein engineering. *Curr. Opin. Biotechnol. 14*, 603−609.
(22) Moatsou, D., Li, J., Ranji, A., Pitto-Barry, A., Ntai, I., Jewett, M. C., and O'Reilly, R. K. (2015) Self-assembly of temperature-responsive protein-polymer bioconjugates. *Bioconjugate Chem. 26*, 1890−1899.
(23) Miserez, A., Weaver, J. C., Pedersen, P. B., Schneeberk, T., Hanlon, R. T., Kisailus, D., and Birkedal, H. (2009) Microstructural and biochemical characterization of the nanoporous sucker rings from Dosidicus gigas. *Adv. Mater. 21*, 401−406.
(24) Guerette, P. A., Hoon, S., Ding, D., Amini, S., Masic, A., Ravi, V., Venkatesh, B., Weaver, J. C., and Miserez, A. (2014) Nano-confined β-sheets mechanically reinforce the supra-biomolecular network of robust squid Sucker Ring Teeth. *ACS Nano 8*, 7170−7179.
(25) Latza, V., Guerette, P. A., Ding, D., Amini, S., Kumar, A., Schmidt, I., Keating, S., Oxman, N., Weaver, J. C., Fratzl, P., Miserez, A., and Masic, A. (2015) Multi-scale thermal stability of a hard thermoplastic protein-based material. *Nat. Commun. 6*, 8313.
(26) Kumar, A., Mohanram, H., Kong, K. W., Goh, R., Hoon, S., Lescar, J., and Miserez, A. (2018) Supramolecular propensity of suckerin proteins is driven by β-sheets and aromatic interactions as revealed by solution NMR. *Biomater. Sci. 6*, 2440−2447.
(27) Hiew, S. H., Guerette, P. A., Zvarec, O. J., Phillips, M., Zhou, F., Su, H., Pervushin, K., Orner, B. P., and Miserez, A. (2016) Modular peptides from the thermoplastic squid sucker ring teeth form amyloid-like cross-β supramolecular networks. *Acta Biomater. 46*, 41−54.
(28) Pena-Francesch, A., Florez, S., Jung, H., Sebastian, A., Albert, I., Curtis, W., and Demirel, M. C. (2014) Materials fabrication from native and recombinant thermoplastic squid proteins. *Adv. Funct. Mater. 24*, 7401−7409.
(29) Cantaert, B., Ding, D., Rieu, C. C., Petrone, L., Hoon, S., Kock, K. H., and Miserez, A. (2015) Stable Formation of Gold Nanoparticles onto Redox-Active Solid Biosubstrates Made of Squid Suckerin Proteins. *Macromol. Rapid Commun. 36*, 1877−1883.
(30) Buck, C. C., Dennis, P. B., Gupta, M. K., Grant, M. T., Crosby, M. G., Slocik, J. M., Mirau, P. A., Becknell, K. A., Comfort, K. K., and Naik, R. R. (2019) Anion-Mediated Effects on the Size and Mechanical Properties of Enzymatically Crosslinked Suckerin Hydrogels. *Macromol. Biosci. 19*, 1800238.
(31) Ding, D., Guerette, P. A., Fu, J., Zhang, L., Irvine, S. A., and Miserez, A. (2015) From Soft Self-Healing Gels to Stiff Films in Suckerin-Based Materials Through Modulation of Crosslink Density and β-Sheet Content. *Adv. Mater. 27*, 3953−3961.
(32) Ping, Y., Ding, D., Ramos, R. A. N. S., Mohanram, H., Deepankumar, K., Gao, J., Tang, G., and Miserez, A. (2017) Supramolecular β-Sheets Stabilized Protein Nanocarriers for Drug Delivery and Gene Transfection. *ACS Nano 11*, 4528−4541.
(33) Ding, D., Guerette, P. A., Hoon, S., Kong, K. W., Cornvik, T., Nilsson, M., Kumar, A., Lescar, J., and Miserez, A. (2014) Biomimetic Production of Silk-Like Recombinant Squid Sucker Ring Teeth Proteins. *Biomacromolecules 15*, 3278−3289.
(34) Davis, L., and Chin, J. W. (2012) Designer proteins: applications of genetic code expansion in cell biology. *Nat. Rev. Mol. Cell Biol. 13*, 168−182.
(35) Xie, J., and Schultz, P. G. (2006) A chemical toolkit for proteins — an expanded genetic code. *Nat. Rev. Mol. Cell Biol. 7*, 775−782.
(36) Sletten, E. M., and Bertozzi, C. R. (2009) Bioorthogonal chemistry: Fishing for selectivity in a sea of functionality. *Angew. Chem., Int. Ed. 48*, 6974−6998.
(37) Davis, M. E., Chen, Z., and Shin, D. M. (2008) Nanoparticle therapeutics: An emerging treatment modality for cancer. *Nat. Rev. Drug Discovery 7*, 771−782.
(38) Keten, S., Xu, Z., Ihle, B., and Buehler, M. J. (2010) Nanoconfinement controls stiffness, strength and mechanical toughness of beta-sheet crystals in silk. *Nat. Mater. 9*, 359−367.
(39) Frottin, F., Martinez, A., Peynot, P., Mitra, S., Holz, R. C., Giglione, C., and Meinnel, T. (2006) The proteomics of N-terminal methionine cleavage. *Mol. Cell. Proteomics 5*, 2336−2349.
(40) Xiao, Q., Zhang, F., Nacev, B. A., Liu, J. O., and Pei, D. (2010) Protein N-terminal processing: substrate specificity of Escherichia coli and human methionine aminopeptidases. *Biochemistry 49*, 5588−5599.
(41) Amiram, M., Haimovich, A. D., Fan, C., Wang, Y. S. S., Aerni, H.-R. R., Ntai, I., Moonan, D. W., Ma, N. J., Rovner, A. J., Hong, S. H., Kelleher, N. L., Goodman, A. L., Jewett, M. C., Söll, D., Rinehart, J., and Isaacs, F. J. (2015) Evolution of translation machinery in recoded bacteria enables multi-site incorporation of nonstandard amino acids. *Nat. Biotechnol. 33*, 1272−1279.
(42) Okur, H. I., Hladílková, J., Rembert, K. B., Cho, Y., Heyda, J., Dzubiella, J., Cremer, P. S., and Jungwirth, P. (2017) Beyond the Hofmeister Series: Ion-Specific Effects on Proteins and Their Biological Functions. *J. Phys. Chem. B 121*, 1997−2014.
(43) Lund, M., and Jungwirth, P. (2008) Patchy proteins, anions and the Hofmeister series. *J. Phys.: Condens. Matter 20*, 494218.
(44) Ball, P., and Hallsworth, J. E. (2015) Water structure and chaotropicity: Their uses, abuses and biological implications. *Phys. Chem. Chem. Phys. 17*, 8297−8305.
(45) Lammel, A. S., Hu, X., Park, S. H., Kaplan, D. L., and Scheibel, T. R. (2010) Controlling silk fibroin particle features for drug delivery. *Biomaterials 31*, 4583−4591.
(46) Chi, E. Y., Krishnan, S., Randolph, T. W., and Carpenter, J. F. (2003) Physical stability of proteins in aqueous solution: Mechanism and driving forces in nonnative protein aggregation. *Pharm. Res. 20*, 1325−1336.
(47) Owczarz, M., and Arosio, P. (2014) Sulfate anion delays the self-assembly of human insulin by modifying the aggregation pathway. *Biophys. J. 107*, 197−207.
(48) Wang, Q., Xia, X., Huang, W., Lin, Y., Xu, Q., and Kaplan, D. L. (2014) High throughput screening of dynamic silk-elastin-like protein biomaterials. *Adv. Funct. Mater. 24*, 4303−4310.
(49) Meyer, D. E., and Chilkoti, A. (1999) Purification of recombinant proteins by fusion with thermally-responsive polypeptides. *Nat. Biotechnol. 17*, 1112−1115.
(50) Zangi, R. (2010) Can salting-In/Salting-Out ions be classified as chaotropes/kosmotropes? *J. Phys. Chem. B 114*, 643−650.

https://dx.doi.org/10.1021/acssynbio.0c00442
ACS Synth. Biol. 2020, 9, 3388−3399

(51) Cao, Z., Chen, X., Yao, J., Huang, L., and Shao, Z. (2007) The preparation of regenerated silk fibroin microspheres. *Soft Matter 3*, 910−915.
(52) Mai, Y., and Eisenberg, A. (2012) Self-assembly of block copolymers. *Chem. Soc. Rev. 41*, 5969−5985.
(53) Molino, N. M., and Wang, S. W. (2014) Caged protein nanoparticles for drug delivery. *Curr. Opin. Biotechnol. 28*, 75−82.
(54) Rossin, R., Versteegen, R. M., Wu, J., Khasanov, A., Wessels, H. J., Steenbergen, E. J., Ten Hoeve, W., Janssen, H. M., Van Onzen, A. H. A. M., Hudson, P. J., and Robillard, M. S. (2018) Chemically triggered drug release from an antibody-drug conjugate leads to potent antitumour activity in mice. *Nat. Commun. 9*, 1−11.
(55) Kaminskas, L. M., McLeod, V. M., Porter, C. J. H., and Boyd, B. J. (2012) Association of chemotherapeutic drugs with dendrimer nanocarriers: An assessment of the merits of covalent conjugation compared to noncovalent encapsulation. *Mol. Pharmaceutics 9*, 355−373.
(56) Costa, S. A., Mozhdehi, D., Dzuricky, M. J., Isaacs, F. J., Brustad, E. M., and Chilkoti, A. (2019) Active targeting of cancer cells by nanobody decorated polypeptide micelle with bio-orthogonally conjugated drug. *Nano Lett. 19*, 247−254.
(57) Martin, R. W., Des Soye, B. J., Kwon, Y. C., Kay, J., Davis, R. G., Thomas, P. M., Majewska, N. I., Chen, C. X., Marcum, R. D., Weiss, M. G., Stoddart, A. E., Amiram, M., Ranji Charna, A. K., Patel, J. R., Isaacs, F. J., Kelleher, N. L., Hong, S. H., and Jewett, M. C. (2018) Cell-free protein synthesis from genomically recoded bacteria enables multisite incorporation of noncanonical amino acids. *Nat. Commun. 9*, 1203.
(58) Carlsen, A., and Lecommandoux, S. (2009) Self-assembly of polypeptide-based block copolymer amphiphiles. *Curr. Opin. Colloid Interface Sci. 14*, 329−339.
(59) Han, G., Wang, J. T., Ji, X., Liu, L., and Zhao, H. (2017) Nanoscale Proteinosomes Fabricated by Self-Assembly of a Supramolecular Protein-Polymer Conjugate. *Bioconjugate Chem. 28*, 636−641.
(60) Huang, W., Krishnaji, S., Tokareva, O. R., Kaplan, D., and Cebe, P. (2017) Tunable crystallization, degradation, and self-assembly of recombinant protein block copolymers. *Polymer 117*, 107−116.
(61) Muiznieks, L. D., and Keeley, F. W. (2017) Biomechanical Design of Elastic Protein Biomaterials: A Balance of Protein Structure and Conformational Disorder. *ACS Biomater. Sci. Eng. 3*, 661−679.
(62) Sun, H., Luo, Q., Hou, C., and Liu, J. (2017) Nanostructures based on protein self-assembly: From hierarchical construction to bioinspired materials. *Nano Today 14*, 16−41.
(63) Huang, X., Li, M., Green, D. C., Williams, D. S., Patil, A. J., and Mann, S. (2013) Interfacial assembly of protein-polymer nano-conjugates into stimulus-responsive biomimetic protocells. *Nat. Commun. 4*, 2239.
(64) Obermeyer, A. C., and Olsen, B. D. (2015) Synthesis and application of protein-containing block copolymers. *ACS Macro Lett. 4*, 101−110.
(65) Araújo, A., Olsen, B. D., and Machado, A. V. (2018) Engineering elastin-like polypeptide-poly (ethylene glycol) multiblock physical networks. *Biomacromolecules 19*, 329−339.
(66) Amiram, M., Quiroz, F. G., Callahan, D. J., and Chilkoti, A. (2011) A highly parallel method for synthesizing DNA repeats enables the discovery of smart protein polymers. *Nat. Mater. 10*, 141−148.

https://dx.doi.org/10.1021/acssynbio.0c00442
ACS Synth. Biol. 2020, 9, 3388−3399